

Electric field control of nonvolatile four-state magnetization at room temperature

Sae Hwan Chun,^{1*} Yi Sheng Chai,^{1*} Byung-Gu Jeon,¹ Hyung Joon Kim,¹ Yoon Seok Oh,¹ Ingyu Kim,¹ Hanbit Kim,¹ Byeong Jo Jeon,¹ So Young Haam,¹ Ju-Young Park,¹ Suk Ho Lee,¹ Jae-Ho Chung,² Jae-Hoon Park,³ and Kee Hoon Kim^{1†}

¹*CeNSCMR, Department of Physics and Astronomy, Seoul National University, Seoul 151-747, Korea*

²*Department of Physics, Korea University, Seoul 136-713, Korea*

³*Department of Physics and Division of Advanced Materials Science, POSTECH, Pohang 790-784, Korea*

*These authors contributed equally to this work.

†To whom correspondence should be addressed; E-mail: khkim@phya.snu.ac.kr

Abstract

We find the realization of large converse magnetoelectric (ME) effects at room temperature in a multiferroic hexaferrite $\text{Ba}_{0.52}\text{Sr}_{2.48}\text{Co}_2\text{Fe}_{24}\text{O}_{41}$ single crystal, in which rapid change of electric polarization in low magnetic fields (about 5 mT) is coined to a large ME susceptibility of 3200 ps/m. The modulation of magnetization then reaches up to $0.62 \mu_{\text{B}}/\text{f.u.}$ in an electric field of 1.14 MV/m. We find further that four ME states induced by different ME poling exhibit unique, nonvolatile magnetization versus electric field curves, which can be described by an effective free energy with a distinct set of ME coefficients.

The capability of the electrical control of magnetization at room temperature becomes increasingly important for many contemporary or next-generation devices such as a multi-bit memory [1] or a novel spintronics apparatus [2]. Multiferroics, in which magnetism and ferroelectricity coexist and couple to each other, could be the most plausible candidates to expect such a converse ME effect via their gigantic ME coupling that generally covers both linear and nonlinear effects [3-8]. Indeed, the vibrant multiferroics research during the past decade has led to significant advances such as the discovery of BiFeO₃ with large electric polarization P [9] and numerous magnetic ferroelectrics allowing sensitive P control by a magnetic field H [3, 4, 10-12]. However, when the general magnetoelectric susceptibility (MES), dP/dH , is evaluated at room temperature, a BiFeO₃ single crystal exhibits the maximum MES less than 55 ps/m (at $\mu_0 H \leq 16$ T) [13]. Furthermore, most of the magnetic ferroelectrics indeed show the giant ME coupling far below room temperature. Although a recent discovery of the room-temperature ME effect in a polycrystalline Sr₃Co₂Fe₂₄O₄₁ has greatly increased the operation temperature, its maximum MES of 250 ps/m [12] is still not enough to expect a significant converse effect. Moreover, even the well-known magnetoelectrics such as Cr₂O₃ [14] and GaFeO₃ [15] did not show substantial modulation of bulk magnetization M by an electric field E at room temperature, mainly due to their weak ME coupling strengths ($dP/dH \leq 5$ ps/m). Therefore, the large room-temperature modulation of M by E still remains as one of great challenges that should be realized in multiferroic or magnetoelectric compounds [16-18].

To overcome the long-standing challenge, we focus here the Co₂Z-type hexaferrite (Ba,Sr)₃Co₂Fe₂₄O₄₁, which consists of a series of tetrahedral and octahedral Fe/Co layers stacked along the c axis ($\parallel [001]$) [Fig. 1(a)]. Sr₃Co₂Fe₂₄O₄₁ is known to have a collinear ferrimagnetic ordering below 670 K, in which the net magnetic moments in alternating large (L -) and small (S -) blocks are oriented parallel to the c axis but antiparallel to each other ($\mu_L > \mu_S$). These moments rotate away from the c axis towards the ab plane below 500 K. The ME effect appears below 400

K where a transverse conical magnetic order appears with the spin propagation vector $\vec{k}_0 = (0, 0, 1)$ [Fig. 1(b)] [19]. As the room-temperature ME effect was realized only in a polycrystalline $\text{Sr}_3\text{Co}_2\text{Fe}_{24}\text{O}_{41}$, we have then tried to grow single crystals of $(\text{Ba,Sr})_3\text{Co}_2\text{Fe}_{24}\text{O}_{41}$ to increase the MES by either controlling directions of electric/magnetic dipoles or by tuning the chemical pressure. In this Letter, we report the first successful single crystal growth of $\text{Ba}_{3-x}\text{Sr}_x\text{Co}_2\text{Fe}_{24}\text{O}_{41}$ in a broad x range. Furthermore, we discover significant converse ME effects at room temperature in a single crystal showing the highest MES, and further show that the compound can save four distinct $M(E)$ curves in a non-volatile way via independent ME writing conditions.

$\text{Ba}_{3-x}\text{Sr}_x\text{Co}_2\text{Fe}_{24}\text{O}_{41}$ ($2.40 \leq x \leq 3.00$) single crystals were grown by the flux method and a $\text{Ba}_{0.52}\text{Sr}_{2.48}\text{Co}_2\text{Fe}_{24}\text{O}_{41}$ single crystal showing the highest MES was selected for the present study [20]. Superior to other hexaferrites [10, 11, 21-23], the $\text{Ba}_{0.52}\text{Sr}_{2.48}\text{Co}_2\text{Fe}_{24}\text{O}_{41}$ crystal exhibits quite high resistivity upon heat treatment [22] ($2.5 \times 10^9 \Omega \text{ cm}$ at 300 K and $1.0 \times 10^7 \Omega \text{ cm}$ at 380 K), which allows successful P evaluations up to 420 K by the MES measurement. The M curves measured at either $\mu_0 H = 50$ or 500 mT [Fig. 1(c)] further indicate that the ferrimagnetic order starts to develop at 680 K and magnetic easy axis changes at 490 K, followed by the stabilization of the transverse conical spin order below $T_{\text{con}} = 410$ K [20]. Our independent neutron diffraction study on the $\text{Ba}_{0.52}\text{Sr}_{2.48}\text{Co}_2\text{Fe}_{24}\text{O}_{41}$ crystal revealed the development of $(0, 0, l)$ ($l = \text{odd}$) peaks below T_{con} , proving that the transverse conical spin order (as in Fig. 1(b)) is indeed stabilized as similar to the case of a polycrystalline $\text{Sr}_3\text{Co}_2\text{Fe}_{24}\text{O}_{41}$ [19].

As demonstrated in Fig. 1(d), nontrivial P ($\parallel [100]$) is induced under a transverse H ($\parallel [120]$) in a wide temperature range below $T_{\text{con}} = 410$ K, yielding maximum P values of $32 \mu\text{C}/\text{m}^2$ at 305 K and $77 \mu\text{C}/\text{m}^2$ at 10 K. Note that P rapidly increases in the 5-50 mT range, in which the magnetic hysteresis curves also show sharp, quasi-linear changes [Fig. 1(e)]. This observation suggests that the spin cone axes are probably disordered in zero or small fields, whereas they are

stabilized into transverse cones at $\mu_0 H \geq 50$ mT [Fig. 1(b)]. According to the spin-current model [24-26], where $\vec{P} \propto \sum \vec{k}_0 \times (\vec{\mu}_L \times \vec{\mu}_S)$ and \vec{k}_0 (\parallel [001]) is the spin propagation vector, the transverse cones depicted in Fig. 1(b) allow a finite P (\parallel [100]). Therefore, alignment of the spin rotation axis toward the H direction will greatly enhance P . In a higher H region (> 1 T), in contrast, the transverse conical component will be reduced at the expense of the collinear ferrimagnetic one, eventually suppressing P . On the other hand, a magnified $M(H)$ curve at 305 K reveals a small hysteresis with a remanent $M = 0.34 \mu_B/\text{f.u.}$ and a small coercive field $\mu_0 H_c \approx 0.3$ mT [Fig. 1(e)], consistent with a soft ferrimagnet-like behavior in the H -controlled crossover between the disordered and ordered transverse cone states. The observation of the remanent M indicates that the transverse cone axes might not be completely disordered to contribute also to non-vanishing P even at zero H -bias.

Direct MES measurements with a very small ac field $\mu_0 H_{ac} = 0.02$ mT indeed confirm the non-vanishing P involving the remanent M . Figure 2(a) and 2(b) show the MES data obtained after the ME poling with $+E_p \equiv 230$ kV/m or $-E_p$ under $+\mu_0 H_p \equiv 2$ T. Upon decreasing H , the MES value for $+E_p$ increases to reach a maximum of 3200 ps/m at $\mu_0 H = 10.5$ mT, and then it decreases almost linearly to have finite intercepts in both H (0.25 mT) and dP/dH (-149 ps/m) axes [Fig. 2(b)]. Eventually it reaches a minimum of -2500 ps/m at -10.5 mT. We note that 3200 ps/m is the highest MES value ever observed in multiferroic compounds at room temperature [12-15]. Thus, the $P(H)$ curve, obtained by integrating dP/dH with H for $+E_p$, shows the steepest slope at 10.5 mT [Fig. 2(c)] and the minimum ($P_{\min} \approx 0$) at 0.25 mT [Fig. 2(d)]. At $H=0$, we obtained a finite $P = 0.016 \mu\text{C}/\text{m}^2$. For $-E_p$, the signs of MES as well as of P are reversed to leave once again a finite $P = -0.016 \mu\text{C}/\text{m}^2$ at $H=0$. When the same experiment was repeated upon increasing H after the ME poling process at $-H_p$, the $P(H)$ curve consistently shows a similar sign reversal with change of electric poling direction. These observations support that the spin helicity, which determines sign of the induced P according to the spin-current model, can be controlled by

the electric poling at $\pm H_p$. The finite P at zero H -bias is likely associated with the memory effects in the spin helicity and the in-plane magnetization. The observation of the remanent M and finite P at zero H -bias thus proves that the $\text{Ba}_{0.52}\text{Sr}_{2.48}\text{Co}_2\text{Fe}_{24}\text{O}_{41}$ single crystal is indeed a multiferroic.

In order to utilize the memory effects in the M control, we first employed the ME poling ($+H_p$ & $+E_p$), termed “*state 0*”, in which $+H_p$ is applied under $+E_p$ and then H_p and E_p are turned off sequentially. M (\parallel [120]) was then measured at a fixed, bias H (\parallel M) while applied E (\parallel [100]) is swept slowly in time at a frequency of 0.02 Hz. We found that M varies significantly with the E sweep in a broad H -bias region below 2 T. The largest modulation was indeed observed at a bias $\mu_0 H = 10.5$ mT, at which the MES value becomes the maximum. Figure 2(e) shows that the M modulation at 10.5 mT reaches as large as $|\Delta M \equiv M(E) - M(0)| = 0.62 \mu_B/\text{f.u.}$, which corresponds to the relative change of $|\Delta M|/M(E=0) \approx 6.0$ %. Moreover, the modulation was reproducible for many E -cycles. When the sign of H -bias was reversed (-10.5 mT), we obtained somewhat reduced $|\Delta M| = 0.45 \mu_B/\text{f.u.}$ and $|\Delta M|/M(E=0) \approx 4.6$ % [Fig. 2(f)]. These results are consistent with the smaller absolute MES value at negative H . In addition, as a natural consequence of the high resistivity in this system, the applied E does not generate any significant leakage current, and thus its M modulation brings only extremely small energy dissipation. Therefore, the current result demonstrates nondissipative, repeatable large M control by E at room temperature, significantly larger than the highest repeatable modulation known to date at 15 K ($|\Delta M| < 3 \times 10^{-3} \mu_B/\text{f.u.}$) [16].

The converse ME effect could be further controlled by ME poling and H -bias conditions. The $M(E)$ curves shown in Fig. 2(e) and (f) indeed show asymmetric line shapes, which can be decomposed into linear and quadratic terms of E that are strongly dependent upon the value of H -bias. For the bias $\mu_0 H = 10.5$ mT (-10.5 mT), the $M(E)$ curve shows a positive (negative) linear slope and a negative (positive) quadratic curvature. Remarkably, we found that such asymmetric

M modulation is sustained even without the H -bias after the initial ME poling. The $M(E)$ curve obtained after applying the “state 0” [Fig. 3] shows a larger M modulation in a negative E region except for a hysteresis near zero E , thereby giving a characteristic, asymmetric parabola shape. When the ME poling is changed into $+H_p$ & $-E_p$ (state 1), the $M(E)$ curve exhibits clearly different parabola shape with a larger M modulation in a positive E region. When the same experiment was repeated with different ME poling of $-H_p$ & $+E_p$ (state 2) or $-H_p$ & $-E_p$ (state 3), the $M(E)$ loops display their own characteristic line shapes, distinguished from the loops for the state 0 or 1. As the result, the four ME poling conditions produce distinct four $M(E)$ loops. Moreover, we also found that all the $M(E)$ loops are persistently repeatable for many E -cycles, proving that the ME information is non-volatile and cannot be erased by the application of E [20]. These results suggest a unique opportunity to store nonvolatile, two-bit information in this single crystal; not only these four states can be written but also can be read by the independent, four M values under a small E -bias. Moreover, under finite $\pm E$ -biases, each asymmetric $M(E)$ curve displays two independent M values. This observation also suggests yet another possibility to store eight different states of M or four-bit information into this material under a finite E .

The $M(E)$ curves in a low H -bias suggest that each curve can be effectively described by a free energy $F(E, H)$ [5],

$$F(E, H) = -PE - \mu_0 MH + \frac{1}{2} \varepsilon_0 \varepsilon E^2 + \frac{1}{2} \mu_0 \mu H^2 + \alpha EH + \frac{1}{2} \beta EH^2 + \gamma E^2 H + \frac{1}{2} \pi E^2 H^2 + \dots$$

, where ε and μ (ε_0 and μ_0) are dielectric permittivity and magnetic permeability of a material (vacuum) and α , β , γ and π are the linear and higher order ME coefficients. By minimizing F with respect to H , the modulations of M with E and H can be described as:

$$\mu_0 \Delta M(E, H) \equiv \mu_0 \{M(E, H) - M(0, H)\} = (\alpha + \beta H)E + (\gamma + \pi H)E^2 + \dots \quad (1),$$

which indicates that the derived $\Delta M(E, H)$ can be approximated by a sum of linear and quadratic E terms in a low E region, being consistent with observations of an asymmetric line shape in the $M(E)$ curves [Figs. 2 and 3]. Eq. (1) further suggests that the coefficients of these linear and quadratic E terms should be linearly dependent upon the H -bias. To check this for each ME state [Fig. 4(a)-(d)], we fitted experimental $\Delta M(E, H)$ vs. E curves at different H -biases ($|\mu_0 H| \leq 10.5$ mT) with Eq. (1).

Figure 4(e) and (f) summarize thus determined coefficients of linear and quadratic E terms (C_1 and C_2) vs. H -bias, respectively. Both coefficients are indeed approximately linear in H especially near $H=0$, and we fitted the curves in Fig. 4(e) (Fig. 4(f)) with a functional form of $\alpha + \beta H$ ($\gamma + \pi H$) to determine the ME coefficients α , β , γ and π for each ME state [20]. We notice that the resultant ME coefficients have almost the same magnitudes but characteristic signs for different ME states. This directly proves that the written ME states can be described by a distinct set of ME coefficients. Moreover, both direct ME and converse ME effects at 305 K can appear in accordance with those stored ME states. It is further inferred that the microscopic parameters such as spin helicity, cone shape, and net spin direction can be also uniquely determined for each ME state, which is characterized by a unique set of the ME coefficients. Therefore, we expect that further understanding on the relationship between the microscopic spin configuration and those ME coefficients are likely to help optimizing the converse ME effects at room temperature.

In summary, we demonstrated the large bulk magnetization modulation by an electric field at room temperature in the hexaferrite $\text{Ba}_{0.52}\text{Sr}_{2.48}\text{Co}_2\text{Fe}_{24}\text{O}_{41}$ crystal. Four independent magnetization vs. electric field curves, generated by the ME poling process, represent four different ME states and can be described by a unique set of ME coefficients. Our result provides

a proof of feasibility for utilizing the converse ME effect for a multi-bit memory, and thus may pave a pathway into development of a practical ME device at room temperature.

This work is supported by CRI (2010-0018300), BSR (2009-0083512) programs and the Fundamental R&D program for Core Technology of Materials. J.-H.C. is supported by the BAERI (2010-0017423) and the Nuclear R&D Program (2010-0018369). J.-H.P. is supported by CRI (2009-0081576), WCU (R31-2008-000-10059-0) and LFRIR (2010-00471) programs.

References

1. M. Gajek *et al.*, Nature Mater. **6**, 296 (2007).
2. Y.-H. Chu *et al.*, Nature Mater. **7**, 478 (2008).
3. T. Kimura *et al.*, Nature (London) **426**, 55 (2003).
4. N. Hur *et al.*, Nature (London) **429**, 392 (2004).
5. W. Eerenstein, N. D. Mathur, and J. F. Scott, Nature (London) **442**, 759 (2006).
6. S.-W. Cheong and M. Mostovoy, Nature Mater. **6**, 13 (2007).
7. R. Ramesh and N. A. Spaldin, Nature Mater. **6**, 21 (2007).
8. Y. Tokura and S. Seki, Adv. Mater. **22**, 1554 (2010).
9. J. Wang *et al.*, Science **299**, 1719 (2003).
10. S. Ishiwata *et al.*, Science **319**, 1643 (2008).
11. S. H. Chun *et al.*, Phys. Rev. Lett. **104**, 037204 (2010).
12. Y. Kitagawa *et al.*, Nature Mater. **9**, 797 (2010).
13. M. Tokunaga, M. Azuma, and Y. Shimakawa, J. Phys. Soc. Jpn. **79**, 064713 (2010).
14. D. N. Astrov, Sov. Phys. JETP **11**, 708 (1960).
15. G. T. Rado, Phys. Rev. Lett. **13**, 335 (1964).
16. M. Saito *et al.*, Nature Mater. **8**, 634 (2009).
17. Y. Tokunaga *et al.*, Nature Mater. **8**, 558 (2009).
18. Y. J. Choi, C. L. Zhang, N. Lee, and S.-W. Cheong, Phys. Rev. Lett. **105**, 097201 (2010).
19. M. Soda *et al.*, Phys. Rev. Lett. **106**, 087201 (2011).
20. See supplemental material for the sample preparation, the measurements, and the ME coefficients.
21. T. Kimura, G. Lawes, and A. P. Ramirez, Phys. Rev. Lett. **94**, 137201 (2005).
22. Y. S. Chai *et al.*, New J. Phys. **11**, 073030 (2009).
23. Y. Tokunaga *et al.*, Phys. Rev. Lett. **105**, 257201 (2010).
24. H. Katsura, N. Nagaosa, and A. V. Balatsky, Phys. Rev. Lett. **95**, 057205 (2005).
25. M. Mostovoy, Phys. Rev. Lett. **96**, 067601 (2006).
26. I. A. Sergienko and E. Dagotto, Phys. Rev. B **73**, 094434 (2006).

Figure captions

FIG. 1 (a) The Z-type hexaferrite structure in the hexagonal setting. (b) Schematic illustration of transverse conical spin states realized under a finite H . μ_L and μ_S (arrows) refer to the effective magnetic moment in the L and S blocks. (c) Temperature dependence of $M_{|| [120]}$ and $M_{|| [001]}$ measured at $\mu_0 H = 50$ (dashed) and 500 mT (solid) after the field cool. (d) $P(H)$ curves after ME poling with $+\mu_0 H_p \equiv 2$ T ($|| [120]$) and $+E_p \equiv 230$ kV/m ($|| [100]$). (e) $M(H)$ curves at 10 and 305 K. The inset shows the magnified curve at 305 K.

FIG. 2 (a) H -dependence of MES for $+E_p$ and $-E_p$ cases at 305 K and (b) the same curve magnified near $H = 0$. (c) $P(H)$ curves and (d) the same curves enlarged near $H = 0$. Arrows indicate H -decreasing or increasing runs. (e), (f) $M(E)$ curves under bias $\mu_0 H = 10.5$ & -10.5 mT, respectively, after the ME poling with $+H_p$ and $+E_p$. Each $M(E)$ curve can be decomposed into linear (solid line) and quadratic components (dashed line).

FIG. 3 The $M(E)$ curves at zero H -bias obtained after applying four different ME poling (*states* 0, 1, 2, and 3) as indicated in the inset.

FIG. 4 (a)-(d) $\Delta M(E)$ curves at different H -bias for the four different ME poling conditions (*states* 0-3 in Fig. 3). (e), (f) The coefficients C_1 and C_2 vs. H -bias for *states* 0-3 upon fitting the experimental ΔM curves in (a)-(d) with $\Delta M = C_1 E + C_2 E^2$.

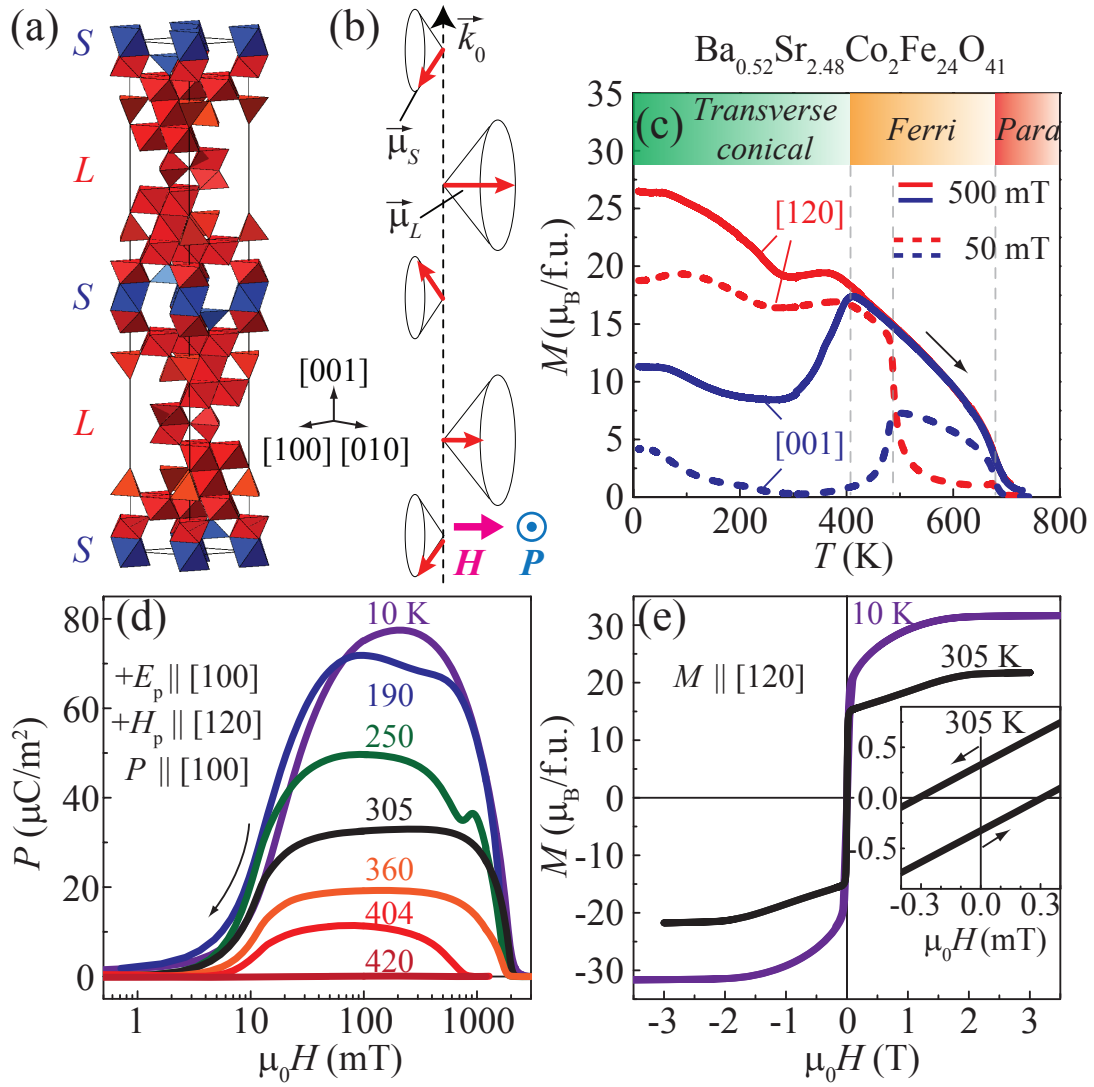


FIG 1. S. H. Chun *et al.*

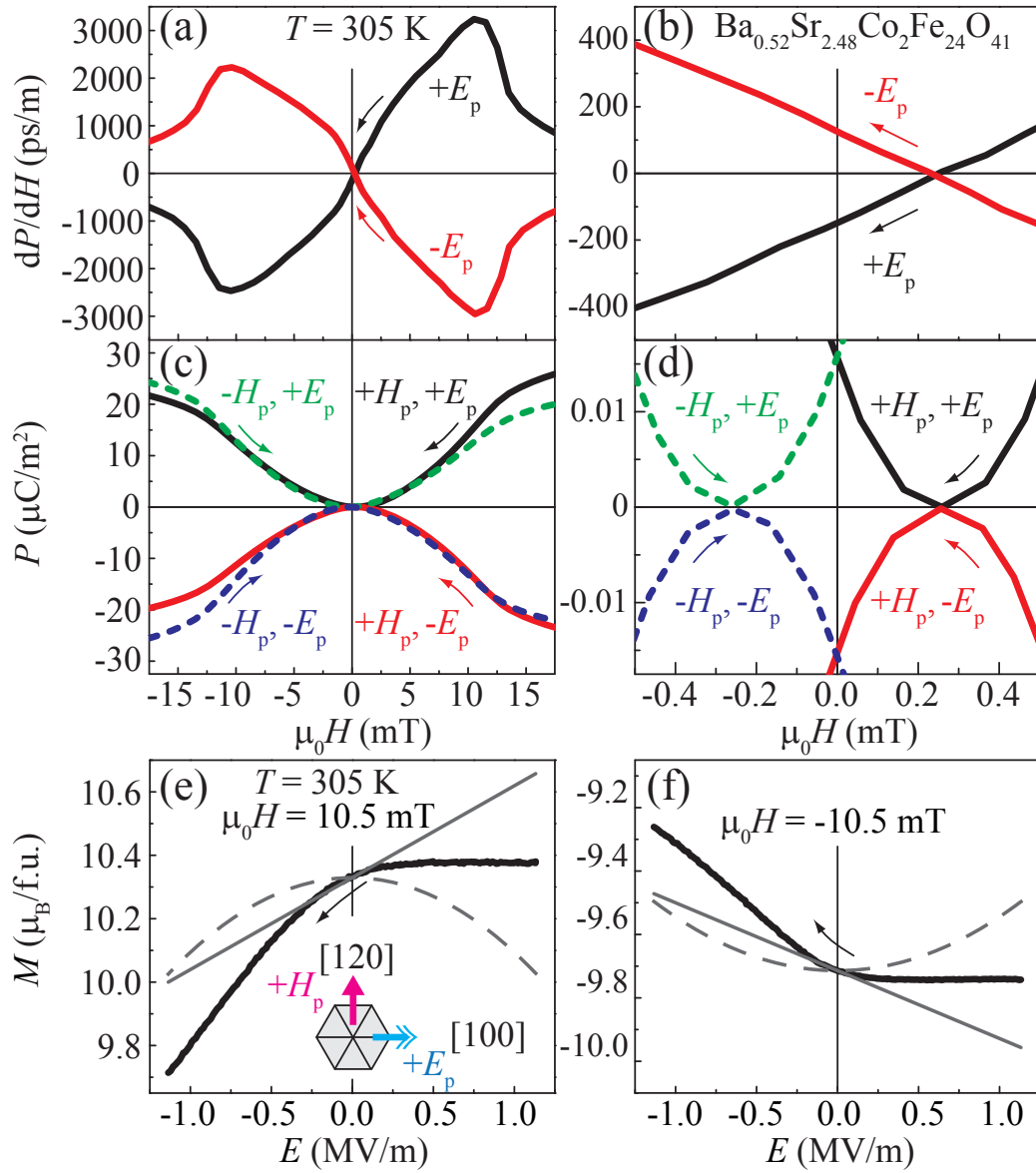


FIG 2. S. H. Chun *et al.*

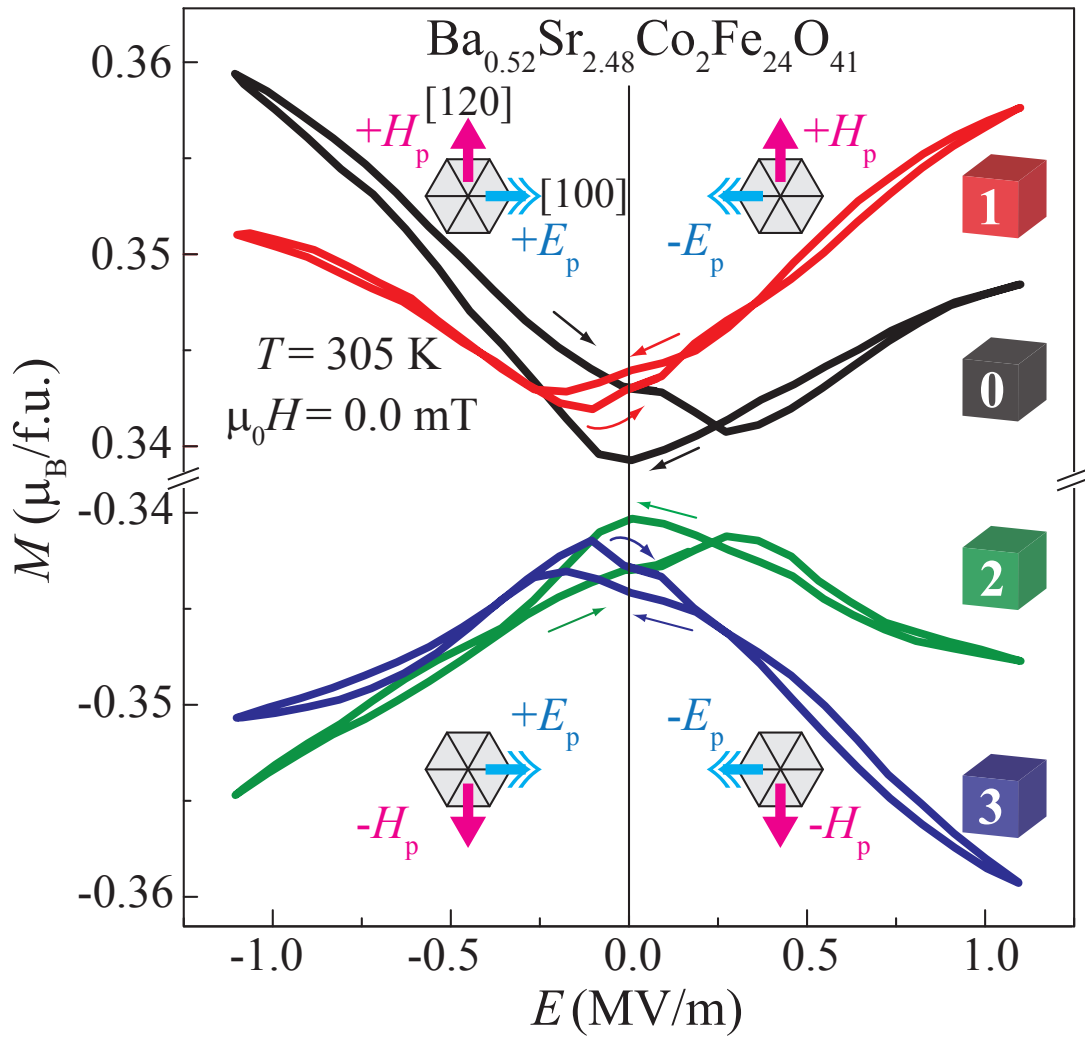


FIG 3. S. H. Chun *et al.*

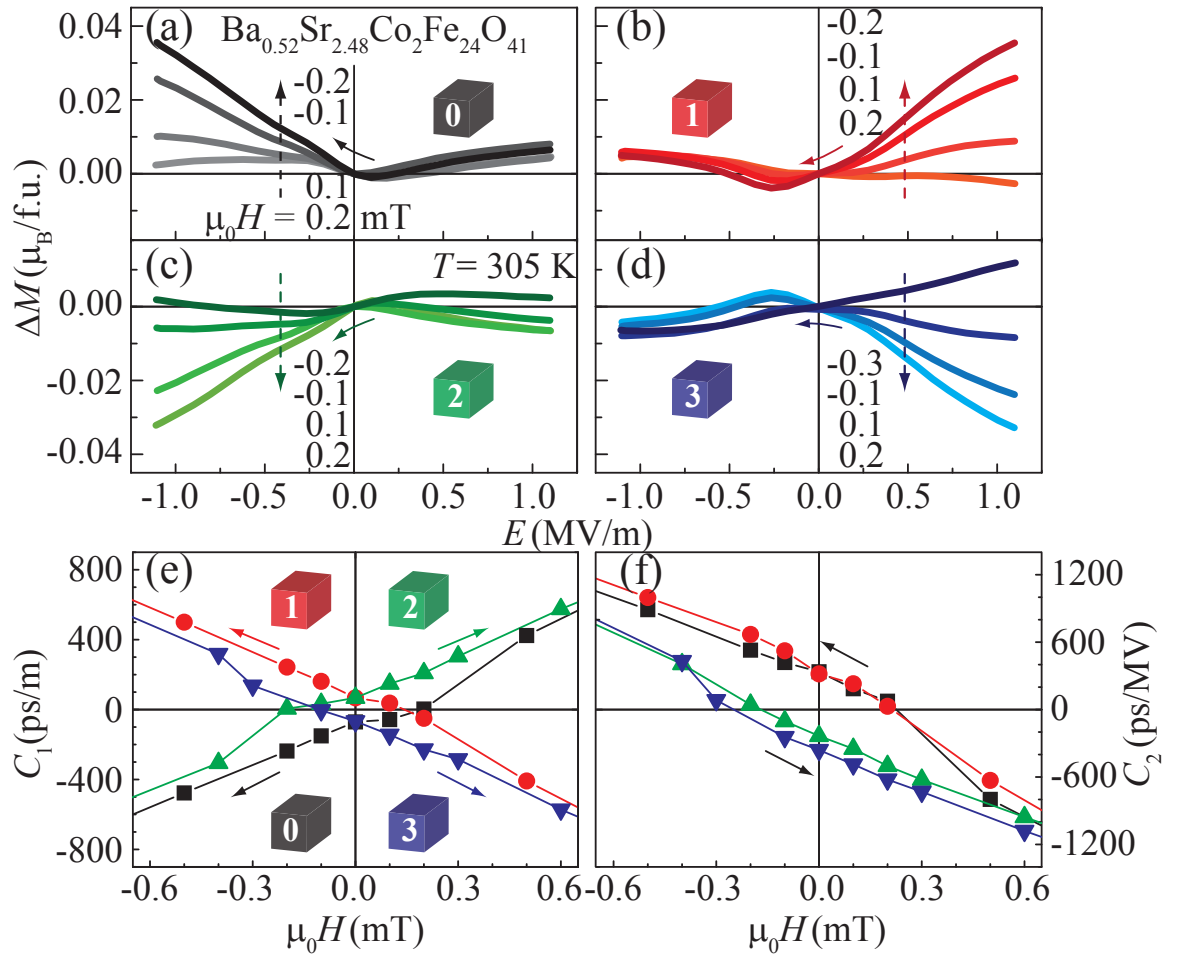


FIG 4. S. H. Chun *et al.*

Supplemental Material for

Electric field control of nonvolatile four-state magnetization at room temperature

Sae Hwan Chun,^{1*} Yi Sheng Chai,^{1*} Byung-Gu Jeon,¹ Hyung Joon Kim,¹ Yoon Seok Oh,¹ Ingyu Kim,¹ Hanbit Kim,¹ Byeong Jo Jeon,¹ So Young Haam,¹ Ju-Young Park,¹ Suk Ho Lee,¹ Jae-Ho Chung,² Jae-Hoon Park,³ and Kee Hoon Kim^{1†}

¹*CeNSCMR, Department of Physics and Astronomy, Seoul National University, Seoul 151-747, Korea*

²*Department of Physics, Korea University, Seoul 136-713, Korea*

³*Department of Physics and Division of Advanced Materials Science, POSTECH, Pohang 790-784, Korea*

*These authors contributed equally to this work.

†To whom correspondence should be addressed; E-mail: khkim@phya.snu.ac.kr

1. Sample preparation

Co₂Z-type Ba_{3-x}Sr_xCo₂Fe₂₄O₄₁ ($2.40 \leq x \leq 3.00$) single crystals were grown from Na₂O-Fe₂O₃ flux in air and heat treated to remove oxygen vacancy at 900 °C under flowing O₂ for 8 days [Ref. S1]. The final product was confirmed to be a single phase using X-ray diffraction on a crushed powder form [Fig. S1]. Chemical compositions of the crystals were determined by electron-probe-micro-analysis (EPMA). The composition was homogeneous over the sample surface within the resolution of the EPMA, and the errors in the determined chemical ratio were about 10 %.

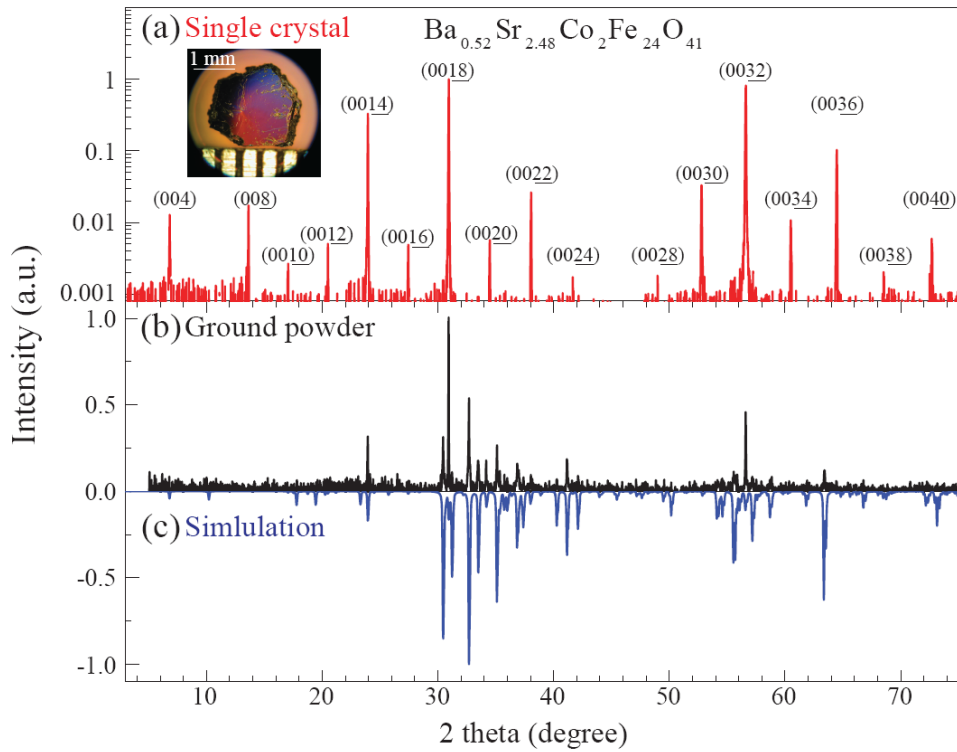


FIG. S1 (a, b) X-ray diffraction patterns of the $\text{Ba}_{0.52}\text{Sr}_{2.48}\text{Co}_2\text{Fe}_{24}\text{O}_{41}$ single crystal and its ground powder, respectively. In (a), the scattering vector was maintained to be parallel to the c axis. (c) A simulated X-ray powder diffraction pattern is also shown for the Z-type crystal with lattice constants $a = 5.867 \text{ \AA}$ and $c = 52.00 \text{ \AA}$ (ICSD #98328). The $(0\ 0\ l)$ peaks for the ground powder show bigger intensities than those obtained by simulation due to the preferential orientation of the partially ground crystallites. The inset shows the picture of a grown Z-type single crystal.

2. Investigations of magnetoelectric and magnetic properties

For electrical measurements, the samples were cut into a rectangular parallelepiped shape with largest surface ($\sim 1 \text{ mm}^2$) normal to the [100] direction. The temperature and the magnetic field were controlled using a Physical Property Measurement System (PPMSTM, Quantum Design). In all the measurements, H was applied along the [120] direction. For MES (dP/dH) measurements, a special solenoid coil is designed to generate ac magnetic field (H_{ac}) modulation of 0.02 mT at a frequency of 171 Hz, which is well compensated not to affect the superconducting magnet in PPMS. The modulated ME charge by H_{ac} is detected by a lock-in amplifier connected through a high impedance charge amplifier with a gain factor of 10^{12} V/C . For accurate phase-sensitive determination of MES signals, the phase of H_{ac} is measured by a voltage pick-up coil inside the solenoid.

The MES and magnetoelectric current were measured and integrated to determine the change of electric polarization with magnetic fields. Before the MES and ME current measurements, the specimen went through a ME poling procedure at 305 K. For $+H_p$ & $+E_p$ poling condition (*state 0*), the sample was kept electrically poled with $+E_p \equiv 230 \text{ kV/m}$ (\parallel [100]) from its paraelectric state at $+\mu_0 H_p \equiv 2 \text{ T}$ (\parallel [120]) to ferroelectric state at 1.2 T. Then, $+E_p$ was turned off and measurements were performed by sweeping H into the paraelectric region, i.e. down to -2 T or up to 2 T. Upon changing the direction of the poled electric field, we could similarly write the *state 1* (i.e., $+H_p$ & $-E_p$). For realizing $-H_p$ & $+E_p$ poling (*state 2*), the sample was kept electrically poled under $+E_p$ while sweeping H from -2 T to -1.2 T, followed by the ME current measurements at zero E -bias. Upon changing the direction of E_p , we could also realize $-H_p$ & $-E_p$ (*state 3*). For P vs. H measurements at different temperatures, the specimen was cooled or warmed to the target temperature after performing a similar ME poling at 305 K. Magnetization curves were measured with a vibrating sample magnetometer (VSM) in the PPMS. To minimize the demagnetization effect, the sample was prepared in a needle-like shape along

the direction of the M measurement. For M vs. E , we modified a conventional VSM sample holder to make the application of high E possible during the M measurement. Particularly for the low H measurement ($|\mu_0 H| \leq 2$ mT), we calibrated H of the superconducting magnet PMS with a standard paramagnetic Pd sample [Ref. S2].

3. Transverse conical state and development of ferroelectricity

The dM/dT curve obtained from the M vs. T curve at $\mu_0 H = 50$ mT clearly shows a dip structure at $T_{\text{con}} = 410$ K, where M (\parallel [001]) vs. T curve under 500 mT starts to decrease upon cooling (Fig. 1(c) in the main text). Both of these features evidence the stabilization of the transverse conical spin order [Fig. S2]. In concurrence with the transverse conical spin order, the electric polarization develops at T_{con} [Fig. S3(a)]. P values at each temperature are determined from the isothermal $P(H)$ curves, which are obtained through the MES measurements for $+E_p$ or $-E_p$ cases. The sign of P changes by reversing the poling E . The dP/dH becomes zero above T_{con} [Fig. S3(b)], supporting again that the electric polarization disappears.

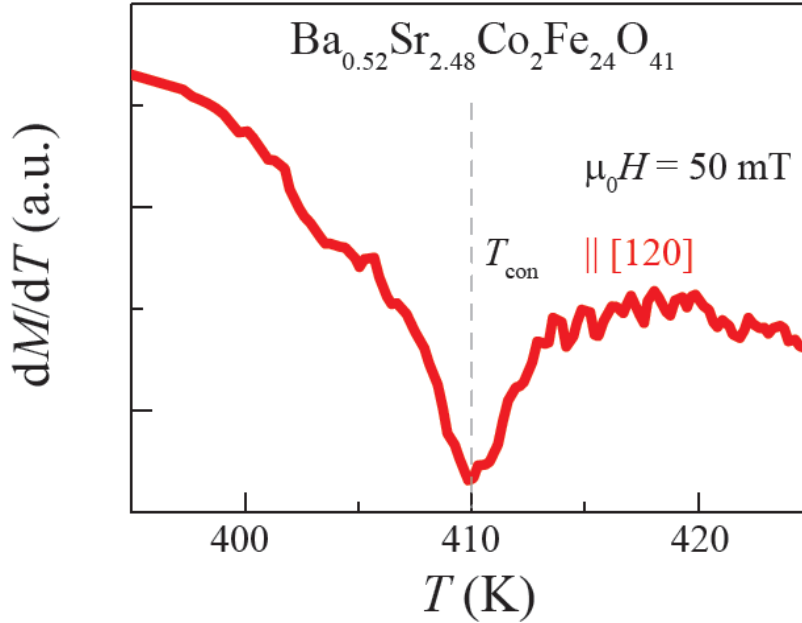


FIG. S2 dM/dT curve estimated from M (\parallel [120]) vs. T curve at $\mu_0 H = 50$ mT.

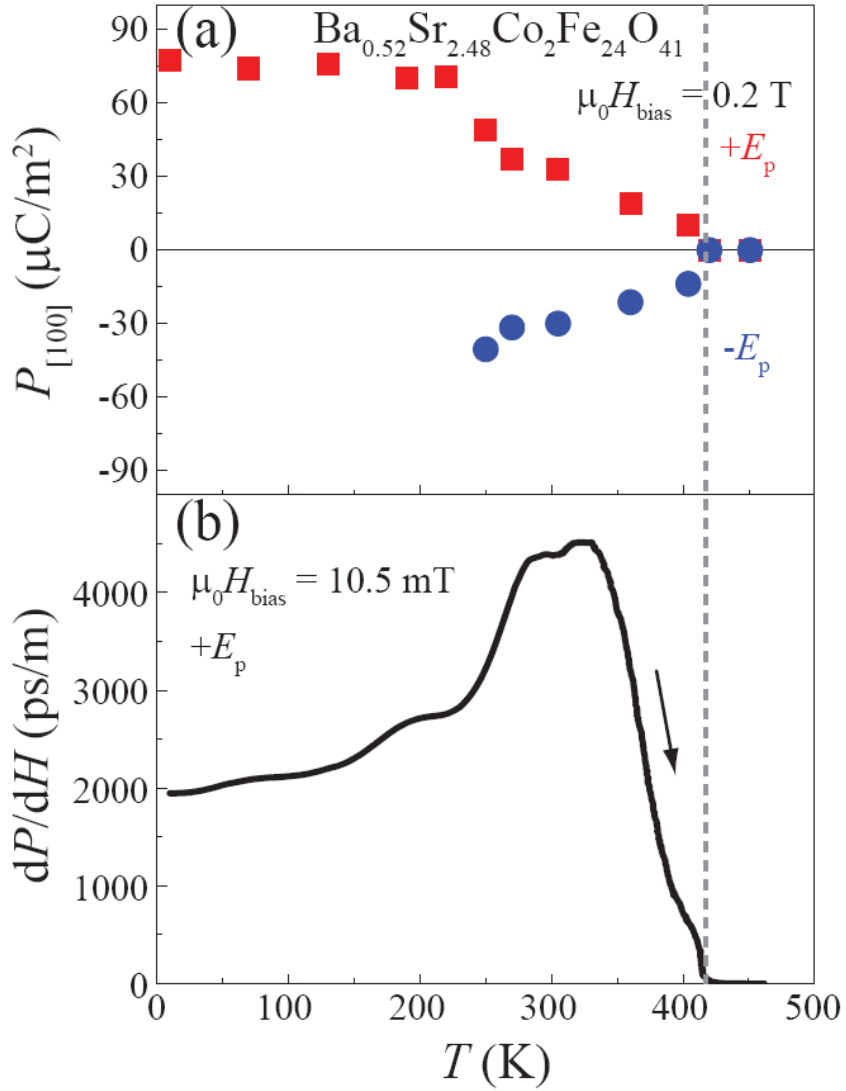


FIG. S3 (a) Temperature-dependence of P at $\mu_0 H_{\text{bias}} = 0.2$ T for different electric poling direction. (b) Temperature-dependence of the MES at $\mu_0 H_{\text{bias}} = 10.5$ mT measured upon warming for a positive electric field poling ($+E_p$).

4. Repeatable magnetization modulation by E at zero H -bias

We herein show that the modulation of magnetization is persistently repeatable for many E -cycles even at zero H -bias. In order to utilize the memory effects in the magnetization control, we first employed each ME poling, termed “*state 0-3*”, in which $\pm\mu_0 H_p \equiv \pm 2$ T is applied under $\pm E_p = \pm 230$ kV/m and then H_p and E_p are turned off sequentially. M (\parallel [120]) was then measured at a fixed, bias H (\parallel [120]) while applied E (\parallel [100]) is swept slowly in time between -1.14 and 1.14 MV/m at a frequency of 0.02 Hz. All the curves, as demonstrated in Fig. S4 (a)-(d), showed quite repeatable traces for many electric field cycles. This experimental result proves that the stored ME information is non-volatile and can be read through repeatable $M(E)$ curves.

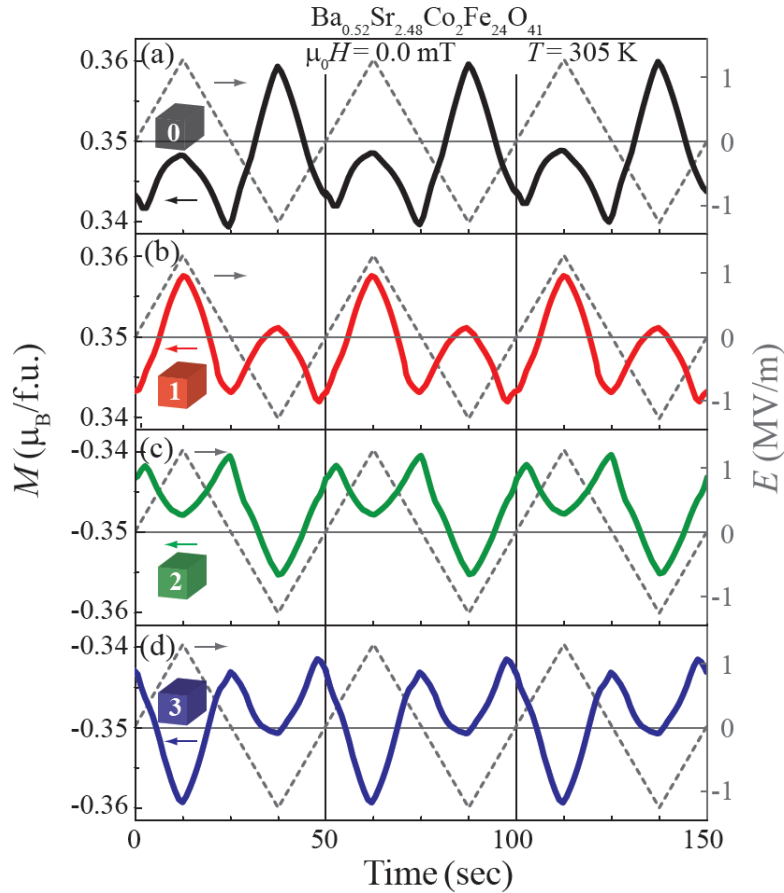


FIG. S4 (a)-(d) Time dependent M variation for each ME state under periodically varying E -bias between -1.14 and 1.14 MV/m (dashed grey) for four ME states (*state 0-3*).

5. Magnetoelectric coefficients

The ME coefficients α , β , γ and π can be extracted from $M(E)$ curves (E -decreasing run) near zero H -bias for each different ME poling condition (Fig. 4(a)-(d) in the main text), as summarized in Table S1.

ME poling	α (ps/m)	β (ps/m·mT)	γ (ps/MV)	π (ps/MV·mT)
State 0 ($+H_p$ & $+E_p$)	-67	467	168	584
State 1 ($+H_p$ & $-E_p$)	67	-622	159	734
State 2 ($-H_p$ & $+E_p$)	67	575	-118	614
State 3 ($-H_p$ & $-E_p$)	-67	-700	-180	608

TABLE S1 ME poling dependence of ME coefficients.

Similar to the ME coefficients extracted from the $M(E)$ curves, the ME coefficients can be directly obtained from the direct MES (dP/dH) measurements as well. Starting from $F(E, H)$ in the main text, minimization of F with respect to E result in the $P(E, H)$ form as followings:

$$P(E, H) = \varepsilon_0 \varepsilon E + \alpha H + \frac{1}{2} \beta H^2 + 2\gamma EH + \pi EH^2 + \dots$$

and then the direct MES for the case of $E = 0$ can be extracted as

$$\frac{dP}{dH}(E = 0, H) = \alpha + \beta H + \dots$$

The experimental data of dP/dH near zero H -bias for each ME poling clearly showed the linear behavior as expected in the above equation and could be thus well fitted with $\alpha + \beta H$, as demonstrated in Fig. S5. Through this procedure, a new set of α and β were obtained as in Table S2.

Careful investigation of Table S1 reveals that the ME coefficients, α , β , and γ , obtained $M(E)$ curves change signs upon changing the written ME states, satisfying the empirical relationship, $\alpha(\pm H_p) \cdot (\pm E_p) < 0$, $\beta(\pm E_p) > 0$ and $\gamma(\pm H_p) < 0$. Furthermore, from the independent, direct MES (dP/dH) measurements for each ME poling [Table S2], we also find that the ME coefficients α and β show similar sign changes. All these experimental results show that the four different ME states can be represented by different set of ME coefficients, and both direct ME and converse ME effects at 305 K can appear in accordance with those stored ME states with the unique set of the ME coefficient.

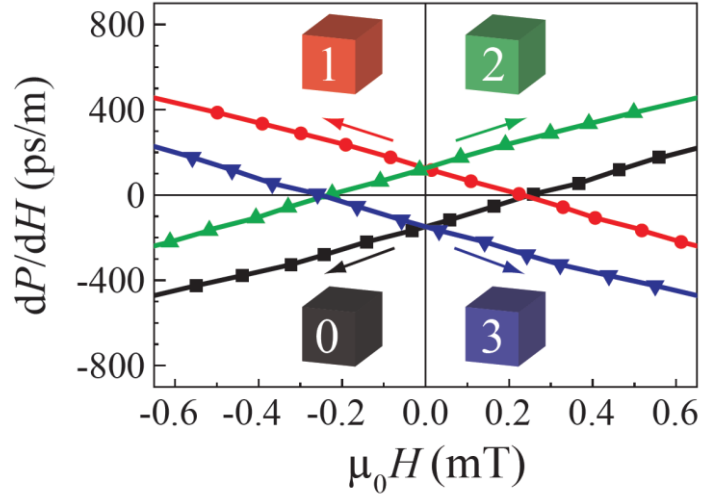


FIG. S5 dP/dH near zero H for four different ME poling conditions.

ME poling	α (ps/m)	β (ps/m·mT)
State 0 ($+H_p$ & $+E_p$)	-149	575
State 1 ($+H_p$ & $-E_p$)	124	-539
State 2 ($-H_p$ & $+E_p$)	124	532
State 3 ($-H_p$ & $-E_p$)	-149	-591

TABLE S2 ME poling dependence of ME coefficients extracted from dP/dH curves in Fig. S5.

References

- S1. Y. S. Chai *et al.*, New J. Phys. **11**, 073030 (2009).
- S2. See, for example, Quantum Design Application Note 1070-207.